Journal of Marine Systems 142 (2015) 96–110

Contents lists available at ScienceDirect

Journal of Marine Systems

journal homepage: www.elsevier.com/locate/jmarsys

# Characterizing observed circulation patterns within a bay using HF radar and numerical model simulations

Fearghal O'Donncha [a,*], Michael Hartnett [b], Stephen Nash [b], Lei Ren [b], Emanuele Ragnoli [a]

[a] IBM Research – Ireland
[b] National University of Ireland, Galway, Ireland

ARTICLE INFO

*Article history:*
Received 12 February 2014
Received in revised form 7 October 2014
Accepted 9 October 2014
Available online 18 October 2014

*Keywords:*
Numerical modelling
Radar
Harmonic analysis
Baroclinic

ABSTRACT

In this study, High Frequency Radar (HFR), observations in conjunction with numerical model simulations investigate surface flow dynamics in a tidally-active, wind-driven bay; Galway Bay situated on the West coast of Ireland. Comparisons against ADCP sensor data permit an independent assessment of HFR and model performance, respectively. Results show root-mean-square (rms) differences in the range $10 - 12cm/s$ while model rms equalled $12 - 14cm/s$. Subsequent analysis focus on a detailed comparison of HFR and model output. Harmonic analysis decompose both sets of surface currents based on distinct flow process, enabling a correlation analysis between the resultant output and dominant forcing parameters. Comparisons of barotropic model simulations and HFR tidal signal demonstrate consistently high agreement, particularly of the dominant M2 tidal signal. Analysis of residual flows demonstrate considerably poorer agreement, with the model failing to replicate complex flows. A number of hypotheses explaining this discrepancy are discussed, namely: discrepancies between regional-scale, coastal-ocean models and globally-influenced bay-scale dynamics; model uncertainties arising from highly-variable wind-driven flows across alarge body of water forced by point measurements of wind vectors; and the high dependence of model simulations on empirical wind-stress coefficients. The research demonstrates that an advanced, widely-used hydro-environmental model does not accurately reproduce aspects of surface flow processes, particularly with regards wind forcing. Considering the significance of surface boundary conditions in both coastal and open ocean dynamics, the viability of using a systematic analysis of results to improve model predictions is discussed.



## 1. Introduction

The coastal ocean represents perhaps the most complex modelling challenge, intimately connected as it is to both the deep ocean and the atmosphere (Song and Haidvogel, 1994). Irregular coastlines and steep and highly variable bottom topography can generate highly complex patterns of flow. Wind forcings produces both surface and internal waves and contributes to surface flows directly through wind drift and Ekman transport. Tidal forcing in addition to barotropic flow processes also includes internal tides, while freshwater discharges add buoyancy fluxes which further complicate water motions locally (Breaker et al., 2004). The presence of a wide ranging set of forcing parameters is particularly true of surface current dynamics encompassing tidal inflow, wind shear, pressure gradients and internal waves (Kim et al., 2009; Ng, 1993; Prandle, 1987, 1997). Consequently, the accurate quantification of flow processes in the upper layers of the ocean is a complex task requiring a holistic consideration of both system forcing variables and accurate field sampling data. A considerable amount of literature has been published involving both numerical model studies (Bryan and Cox, 1968; Davies and Jones, 1992; Price et al., 1987), and in-situ current measurement profiles (Brink, 1991; Munchow and Garvine, 1993) of wind-driven surface flows.

Numerous studies have demonstrated the major effect that wind and meteorological conditions can have on tidal flows. The surface current response to wind is believed to be isotropic in the open ocean in agreement with Ekman theory (Ekman, 1905; Rio and Hernandez, 2003). However, the behaviour of wind-driven flow in coastal regions can be more complex due to the horizontal pressure gradient and frictional resistance exerted by the bottom topography and coastline (Kim et al., 2009; Rabinovich et al., 2007); this can result in anisotropic and asymmetric response of surface currents as the local effects of topography and the frictional balance with wind are not equivalent in the along shore and cross-shore direction (Kim et al., 2011). Consequently, complex circulation patterns and gyre formations can develop within coastal regions that affects both dynamics and nutrient dispersion. Weisberg et al. (2001) investigated coastal shelf circulation patterns in West Florida via numerical model simulations and field data; whereas wind was determined to be the primary motive agent, the accurate simulation of field conditions required that model density fields be maintained. In addition thermal differences resulted in asymmetric flow patterns wherein the scale and magnitude of the offshore

* Corresponding author.
*E-mail address:* feardonn@ie.ibm.com (F. O'Donncha).

http://dx.doi.org/10.1016/j.jmarsys.2014.10.004
0924-7963/

upwelling responses were larger than those for the downwelling responses. The effect that this asymmetry may have on nutrient supply within the region was noted. Pidgeon and Winant (2005) investigated temperature variability and currents on the continental shelf as a result of meteorological conditions and tidal forcing. A surface enhanced vertical mode of temperature variability was detected, while the surface velocity field was dominated by a coherent clockwise component as a direct response to the diurnal heating and wind forcing.

The technology of measuring surface current by high frequency radar (HFR) has been rapidly expanding over the last decade (Yaremchuk and Sentchev, 2011), having been used to study nearshore circulation in a large variety of environmental conditions (Prandle et al., 1993; Kohut et al., 2006; Ullman et al., 2006); Kohut et al., 2008; Lipa et al., 2009. HFR systems have a number of unique advantages in terms of the observation of coastal ocean dynamics. These include: providing real-time data over large ocean areas at relatively low cost; enabling two-dimensional mapping of surface currents at resolutions that capture the complex structure related to coastal bathymetry and the intrinsic instability scales of the coastal circulation; as systematic input to operational ocean models via data assimilation (Paduan and Washburn, 2013); while HFR systems can also play a role in environmental monitoring and event response systems. (O'Donnell et al., 2005) showed that trajectory predictions produced by HFR were approximately a factor of two superior to those produced using present practise in which the advective velocity is obtained from tidal current predictions in nearshore waters and a surface current climatology offshore.

HFR allows measurement along the conductive sea surface for distances of up to 200 km offshore at time intervals of 0.2–1 h (Yaremchuk and Sentchev, 2009). This enables synoptic current maps of surface flows to be produced, which, due to contamination by surface waves are often difficult to obtain by traditional measuring programs (Essen et al., 2000). In addition to their role in coastal observatory systems, these datasets are ideal for the rigorous testing and validation of three-dimensional numerical models; this is particularly true in wind-driven bays and estuaries where HFR measurements provide a unique insight into the effects of wind shear on surface currents.

This paper describes research conducted in assessing circulation patterns via by combination of numerical model, HFR and Acoustic Doppler Current Data (ADCP) data in Galway Bay. A detailed dataset of HFR observed currents was collected at 60 minute intervals for the month of December 2011. In conjunction with this, numerical simulations of the bay using a terrain-following, three-dimensional coastal ocean model were computed.

The study focuses on a holistic investigation of numerical simulations and high resolution observations in a tidally active, high-wind, coastal embayment. It presents the first detailed study of this complex bay hydrodynamics. The pairing of extensive sensor data and complex flow processes induced by the forcing of high winds, irregular topography and large tidal ranges, represents a unique opportunity to comprehensively assess model skill. The focus of this paper is twofold: combining data and model output to better describe circulation processes than would be possible from either in isolation; and subsequently, to isolate sources of error in the model results based on the measured datasets. Analysis of model performance adopts a multi-pronged approach: qualitative aspects of model flows are assessed by measurements of correlation; a quantitative index of agreement proposed by Willmott, (1981) defines model skill; while signal processing techniques enable a further decomposition of both modelled and observed surface currents into the dominant forcing mechanisms. The approach presented enables a systematic analysis of model capabilities in a complex environment, while identifying model shortcomings. Conclusions are drawn regarding the refinement of an advanced, widely-used hydrodynamic model to better simulate surface flow dynamics in a representative coastal environment.

The methodology section presents the approach adopted; this section includes a description of both the HFR system and the numerical model used, and briefly presents the analysis techniques. A short description of the characteristics of Galway Bay is provided and details of model construction and model set-up are provided. The section on results presents a description of the application of the model to the bay; details of the model validation program are outlined. Results of model simulations are presented and systematically compared with HFR observations. Finally, conclusions from this research are drawn and the recommendations for future research made.

## 2. Methodology

### 2.1. Study site

Galway Bay is situated on the West coast of Ireland. It lies between 53°02'N to 53°14'N latitude and 09°00'W to 09°27'W longitude. The bay is approximately 50 km in length and 20 km at its widest. The Aran Islandsextending across the mouth of the bay form a natural land barrier, which protects the bay from the open Atlantic Ocean. The principal islands are separated from each other by, Gregory and Foul sounds, and from the mainland by North and South sounds. These four channels link the Bay with the Atlantic ocean. The North and South Sounds are approximately 13 km wide and have maximum depths of 69m and 57m respectively. Galway Bay can be conveniently divided into an Inner and Outer Bay by an imaginary line joining Spideal on the North Coast to Black Head on the South Coast (Fig. 1). The Inner Bay is shallow, with depths less than 30m; the outer Bay is up to 70m deep in and near the North Sound.

The dynamics within the bay are mainly influenced by: oceanic flows to the bay from the adjacent shelf; freshwater discharges, primarily from the River Corrib; and wind driven currents. Oceanic flows enter the bay mainly through the southern sounds, circulate within the bay before exiting through the North Sound. The water circulation through these sounds influences the physics, chemistry and biology of the waters of the bay (Booth, 1975; Fernandes, 1988). The River Corrib drains approximately 70% of the catchment area around Galway Bay with a mean annual flow of $98.89 m^3/s$ (BIM, 2012), discharging into the Inner Bay and generally extending seawards along the north coast (Nolan, 1997). Exposed to Atlantic weather systems, average wind speeds in January within the bay are $12 ms^{-1}$ and even during the calmest month of June is $7 ms^{-1}$ (Institute, 1999).

Current meter data recorded by Fernandes (1988) during March 1985 showed that the general direction of water through Foul and South sounds, coincided with the tidal current direction, i.e. into Galway Bay, on the flooding tide. However, at Gregory Sound, the flow was found to be into Galway Bay despite sampling at ebb tide. This reverse flows was possibly driven by a north-westerly wind blowing at 5m/s, thus indicating that the wind speed and direction along with tidal effects may be significant factors affecting the entry and exit of water through Gregory Sound and possibly other sounds of Galway Bay.

Booth (1975) and Fernandes (1988) indicated the existence of a circular body of water, likely a gyre, located in the Outer Bay between Spideal and the Aran Islands (see Fig. 1). However the studies differed on the direction of rotation of the water. Booth (1975) proposed a cyclonic gyre that would direct the Corrib humic material, coming along the northern shore of the Bay, towards the North Sound and exiting the bay. Chemistry data collected by Fernandes, (1988), however indicated that humic material was accumulated, suggesting an anti-cyclonic motion. The presence of the gyre and its property of accumulating some of the Corrib waters, indicate that there would in actual fact, be a delay in theflushing time of the waters from Galway bay. These conflicting results emphasize the sparsity of reliable information available on bay circulatory patterns, with much of the knowledge being anecdotal in nature or the result of relatively small-scale field studies.

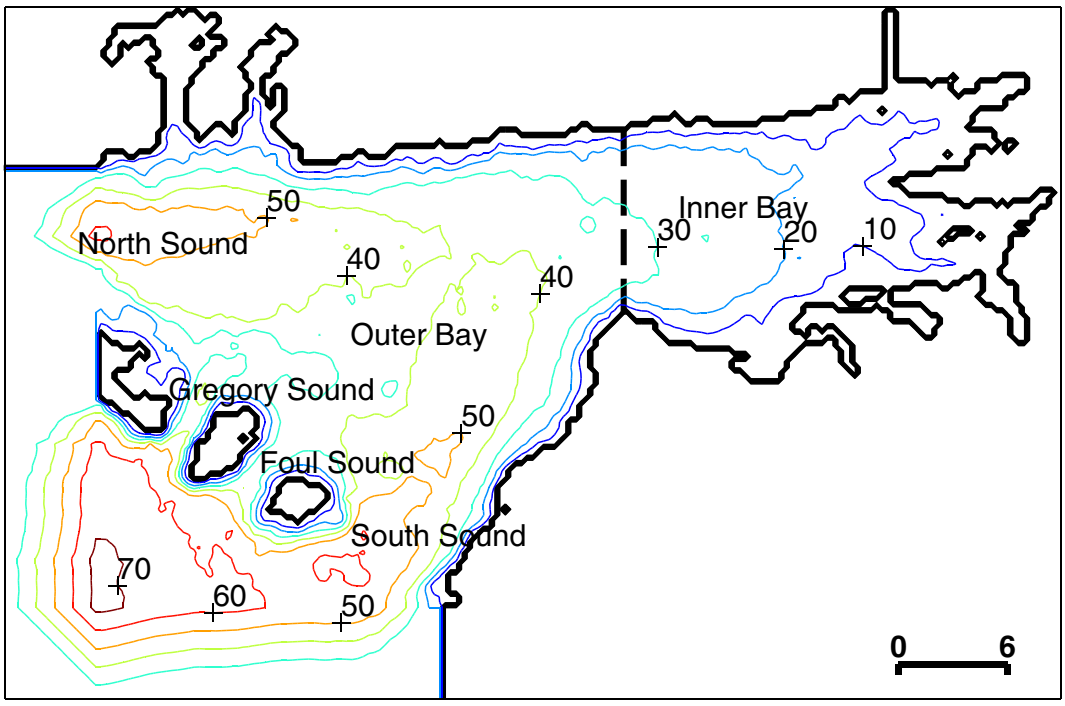


**Fig. 1.** Galway Bay bathymetry contour map denoting main geographic features of the bay along with convenient division between inner and outer bay.

### 2.2. Field measurements

Field measurement centred on HFR measurements from a coastal ocean dynamics applications radar (CODAR) ocean sensors SeaSonde system (Barrick et al., 1977), supplemented by additional instrument deployments. HFR uses the theory of Bragg scatter within a signal peak to calculate radial components of the total surface velocity at a given location. It is based on the fact that radar backscatter from the ocean surface is from Bragg-resonant surface waves; that is, those waves whose wavelength is exactly half the radio wavelength, and that travel exactly toward or away from the radar. The phase speed of the surface waves can then be separated from the total frequency shift using linear wave theory, leaving only that shift due to the surface current. The voltage cross spectra are then analysed using the direction finding MUSIC algorithmto generate radial current maps (Gurgel et al., 1997; Schmidt, 1986). Radial data are collected at 10 minute intervals and then averaged over an hourly time period to produce a radial current map for the observation system. To produce a vector map it is necessary to have two or more overlapping radials. The intersection angle of individual radials is central to constructing reliable current vector fields. This reconstruction limitation is the well known Geometric Dilution of Precision (GDOP), and results when the angle between two

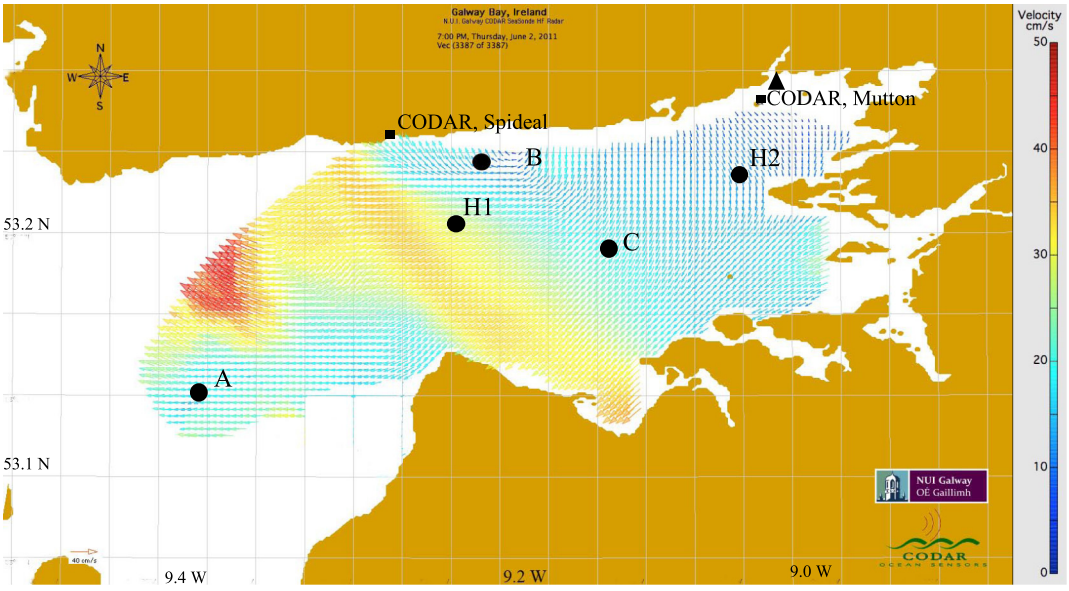


**Fig. 2.** Galway Bay current vector map displaying location of field monitoring sensor suite: two radar sites (site 1 denoted Mutton and site 2 denoted Spideal), tide gauge (black triangle) and ADCPs. Circles A, B and C refer to three ADCPs deployed for extended periods during the study period while H1 and H2 refer to location where point comparisons of model and HFR observations were conducted.

radials is too large to enable accurate resolution of the component perpendicular to the radials (Chapman et al., 1997). GDOP is a coefficient of uncertainty that characterizes the effect of the geometry of the coupled radar system on the measurement and position determination uncertainties (Emery et al., 2004).

The study uses data from two standard-range radar sites installed as part of an integrated coastal ocean observation system in Galway Bay. The location of the two radars, chosen to achieve a practical balance between coverage across the bay and horizontal resolution, is shown in Fig. 2, along with a current vector map displaying a synoptic view of surface flow. The radar operating at a frequency of 25 MHz measures continuous radial vectors at an effective depth of 0.48m (Stewart and Joy, 1974). A sampling range of 25km is provided by the radar with a spatial resolution of 0.3km. The radars were locally calibrated using antenna beam pattern measurements. To minimise erroneous discrepancies in the analysis, only grid points which returned data more than 50% of the time were considered.

Acoustic Doppler Current Profilers (ADCP) deployed at different stages of the study were used to both ground truth the performance of the radar and validate the model. Probe A (Fig. 2) was deployed between 26/09/2011 and 14/11/2011, while probe B was deployed during the preliminary planning stages of the HFR observation project from 01/05/2007 to 13/06/2007. For assesment of HFR accuracy probe C was deployed at the centre of the CODAR footprint for a three month period, July-October 2013. The instruments were configured to profile currents with a vertical resolution (bin size) of 1m and a sampling frequencyof 20 minutes. The instrumentation error of the ADCP itself was not considered as part of this study as they are generally considered quite accurate with error less than a few centimetres per second; a study by (Yoshikawa et al. (2007) comparing two different ADCP measurement reported rms differences of 1.52 *cm/s*. The objectives of the ADCP deployments were twofold: evaluating the accuracy of HFR current measurements; and an assessment of model performance in tidally-dynamic regions of the bay, not covered by HFR monitoring. Hence, probe A was placed at a designated location within the middle bay where Southern and Westerly flows converge and the ability of the model to replicate these complex flow patterns investigated; probe B was positioned close to the Northern Shore where the influences of coastal bathymetry and freshwater discharges were believed to be at their most significant (Booth, 1975); while probe C was deployed at the centre of the HFR measuring footprint.

A weather station located at National University of Ireland, Galway provided meteorological data used to prescribe surface boundary conditions for the model. A range of atmospheric parameters were sampled at ten minute intervals including: temperature, solar radiation, relative humidity and rainfall. To better facilitate comparisons with future studies, wind forcing used in the study was extracted from the operational High Resolution Local Area Modelling (HIRLAM) output at the grid point closest to the centre of the HFR observation grid (53.25° N, 9.25° W). Fig. 3 plots the directional influences of the model winds dataset over the duration of the study period, highlighting the significant South-Westerly bias present in the bay. Freshwater discharges for the River Corrib were specified based on field data sampled at 15 minute intervals.

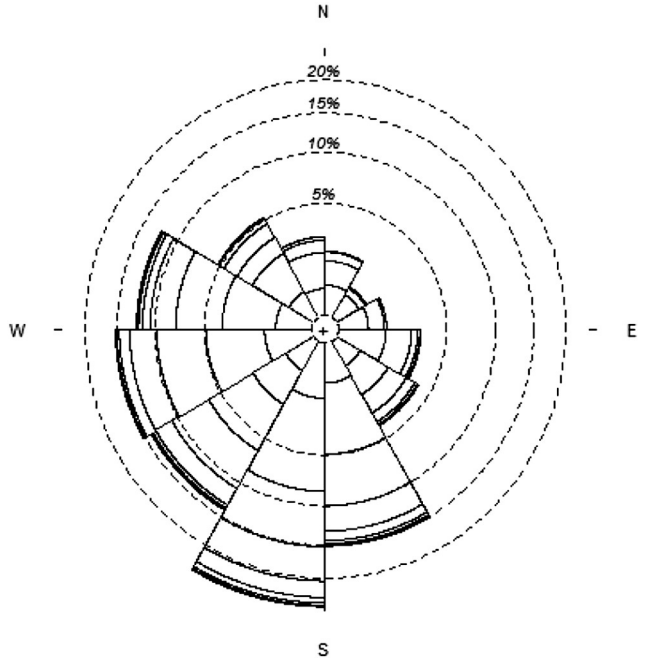


**Fig. 3.** Variation of wind distribution during the study period.

### 2.3. Numerical modelling

The model used for this study was Environmental Fluid Dynamics Code (EFDC), a three-dimensional, finite difference, hydrodynamic model. An outline of this model is presented here and the reader is referred to Hamrick (1992a, 1996) and Ji et al. (2001) for a detailed description of the numerical algorithm.

EFDC is a general-purpose modelling package for simulating three-dimensional flow, transport and biogeochemical processes in surface water systems. It resolves the vertically hydrostatic momentum and continuity equations in a curvilinear coordinates system, orthogonal in the horizontal and sigma-stretched, or terrain-following in the vertical. Three dimensional transport equations for temperature, salinity, dye tracer and suspended sediment are also computed simultaneously. A second-order turbulence closure model developed by Mellor and Yamada (1982) and modified by Galperin et al. (1988) is adopted to provide the vertical turbulent viscosity in the model. Horizontal diffusion is calculated via the Smagorinsky formula (Smagorinsky, 1963).

The computational scheme uses a second-order accurate, three-time-level finite difference scheme with an internal-external mode splitting procedure to separate the internal shear or baroclinic mode from the external free surface gravity wave. The external mode solution uses a semi-implicit scheme that allows large time steps constrained only by the stability criteria of the explicit central difference or upwind advection scheme used for the nonlinear accelerations. Time splitting inherent in the three-time-level scheme is controlled by a periodic insertion of a two-time-level step. The internal mode, associated with vertical shear of the horizontal velocity components is solved using a fractional step scheme combining an implicit step for the vertical shear terms with an explicit formulations for all other terms.

Specifically designed to simulate estuaries and subestuarine components (tributaries, marshes, wet and dry littoral margins), the model has been applied to a wide range of environmental studies in the Chesapeake Bay region (Shen et al., 1999). It has also been applied in a wide range of investigations of other systems including: environmental impact assessment studies (Hamrick, 1992b), salinity transport (Moustafa and Hamrick, 1994), suspended sediment transport (Bai and Lung, 2005), larval transport (Shen et al., 1999) and hydrothermal responses (Khangaonkar et al., 2005). The model is presently being used by universities, research organisations, governmental agencies, and consulting firms (Ji, 2008).

The model was used to analyse circulation patterns within Galway Bay. High-resolution bathymetric data of the bay was obtained from a topographical surveying program conducted by the Irish National Marine Institute as part of the INFOMAR project (Wheeler and Monteys, 2010). These data were interpolated onto a finite difference mesh with grid spaced at 300m interval. A total of 13,000 computational cell were used in the horizontal plane with ten sigma layers being used in the vertical. Extents of the study area are presented in Fig. 1.

The open sea boundaries of the model were the Southern and Western boundaries. There are two types of hydrodynamic open boundary conditions (OBC) available within EFDC model (Hamrick, 1996). The first type uses the standard specification of water surface elevations, using combinations of harmonic constituents and time series. The second type uses the radiation-separation boundary condition. With this type of OBC, the incoming wave at an open boundary is separated from the outgoing wave and the incident wave is assumed to be twice the surface elevation required. By default, the outgoing characteristic is left undefined, allowing waves generated interior to the model domain to pass outward across the boundary with no reflection. During preliminary model simulations both OBCs were compared to assess differences between computed elevations and flows within the domain. Since no noticeable differences resulted the first type of boundary conditions was adopted due to the mathematically simpler implementation. Tidal information from the Oregon State University Tidal Prediction Software (OTPS/TPXO) based on the TOPEX/ POSEIDON altimeter data (Egbert and Erofeeva, 2002; Padman and Erofeeva, 2004) was used to prescribe tidal elevations at the boundaries. Data from a tide gauge deployed at the location shown in Fig. 2, which provided real-time tidal data at 6 minute intervals, were used to fine-tune model elevations. Fig. 4 displays the numerically computed tidal elevations plotted against tide gauge data for a subset of the study period.

### 2.4. Analysis

The main verification and statistical techniques employed during this research consist of: Pearson correlation coefficient, Kundu's vector correlation coefficient, root-mean-square deviation (RMSD) and Willmott's model skill score. These terms are discussed briefly below.

Pearson's product moment correlation coefficient describes colinearity between observed and predicted values (Wilks, 2011). However, as this parameter only evaluates linear relationships between the variables, high values of correlation can be obtained even when the model simulations and observations differ considerably in magnitude. In addition, correlation based measures are more sensitive to outliers than values near the mean (Moore and Notz, 2010); consequently, a model that can replicate extreme events will post artificially high values of correlation (Legates and Davis, 1997).

An alternative metric, that provides measure of the correlation between two vector datasets is the complex correlation coefficient $\rho$, proposed by (Kundu, 1976). Expressing the complex representation of the two-dimensional horizontal velocity vector as:

$$w(t) = u(t) + iv(t) \tag{1}$$

then the complex correlation coefficient between the two datasets $(w_1, w_2)$ is computed as

$$\rho = \frac{< w_1^* w_2 >}{< w_1^* w_1 >^{\frac{1}{2}} < w_2^* w_2 >^{\frac{1}{2}}} \tag{2}$$

where the asterisk indicates the complex conjugate and the angle brackets denote average in time. The quantity $\rho$ is a complex number whose magnitude gives a measure of correlation and whose phase angle, arg($\rho$), gives the average counter-clockwise angle of the second vector with respect to the first (Kundu, 1976).

An absolute measure of model deviation from measured data is the root-mean-square deviation (RMSD) which can be expressed as:

$$RMSD = \sqrt{\frac{\sum_{i=1}^{n} (X_{model} - X_{obs})^2}{n}} \tag{3}$$

where $X_{model}$ and $X_{obs}$ represent the predicted and observed value respectively.

The ability of a model to predict events is often too elusive to be adequately encapsulated by these standardised coefficients of agreement (McCuen and Snyder, 1975). In order to circumvent these difficulties, Willmott, (1981) proposed a model skill score, $d$, to overcome the sensitivity of correlation statistics to differences in the predicted mean and variances (Legates and McCabe, 1999). It can be expressed as:

$$d = 1 - \frac{\sum |X_{model} - X_{obs}|^2}{\sum \left( |X_{model} - \overline{X}_{obs}| + |X_{obs} - \overline{X}_{obs}| \right)^2} \tag{4}$$

where the overbar denotes the mean of the dataset. The highest value, $d = 1$, means perfect agreement between model and observation, while the lowest, $d = 0$, indicates complete disagreement. Skill scores permit greater insights into the predictive abilities of models with allowances for ambient flow speeds and relative MSD. In assessing model performance Legates and McCabe (1999) recommends the inclusion of at least one relative error measure (e.g. model skill score) and one absolute error measure (e.g. RMSD) with additional supporting information. Recently, this index was used to evaluate numerical model results with regards the impacts of different turbulence closure schemes (Warner et al., 2005); the simulation of circulation patterns on the New England shelf (Wilkin, 2006) and the Columbia River estuary (Liu et al., 2009).

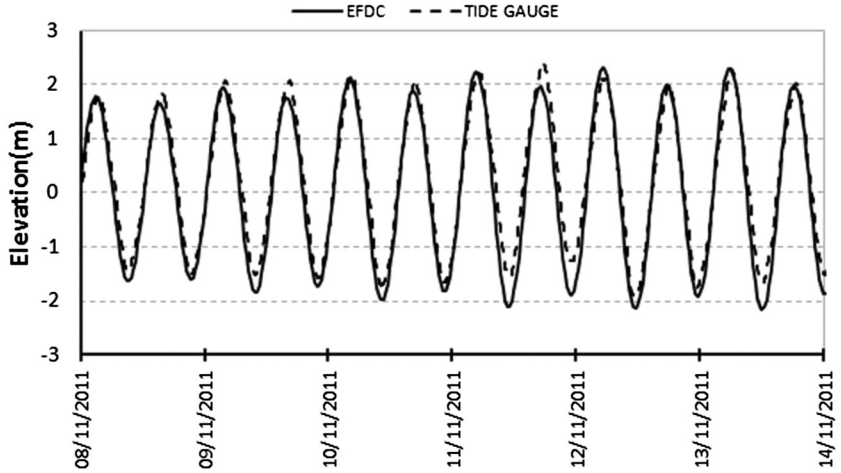


**Fig. 4.** Numerically computed tidal elevations plotted against measured data.

## 3. Results

Analysis of model performance focuses on both point and field scale level. Time series comparisons at selected points enable a visual study of quantitative comparisons, while providing insight into systematic deviations from true state. In conjunction with this, flow-field agreement metrics evaluate model performance across the domain. A further investigation of the current patterns employs a classical tidal analysis approach that allows for a more detailed, statistical assessment of model performance in terms of individual forcing mechanisms.

### 3.1. Time series analysis

Initially ADCP data were compared with model output and HFR surface currents, where model comparisons assessed both surface and vertical profile processes. Prior to analysis, model and sensor data were high pass filtered to eliminate low frequency variations that might contaminate the data comparisons. To obtain high pass filtered data the time series were averaged to hourly intervals, low-pass filtered using a cosine-Lanczos filter with a 40-h halfpower point, and finally the required data extracted by subtracting the low-pass filtered data from the original timeseries (Emery and Thomson, 2001; Kosro, 2003).

An inherent limitation in ADCP current measurements is contamination of data near the surface due to side-lobe contamination and near-surface, wind-induced errors (Marmorino and Hallock, 2001; Teague et al., 2001). Instrumental specifications suggest the depth of contamination to be approximately 15% of the water column (Essen, 1994). To investigate this further and also provide insight on the importance of baroclinic flows to local circulation patterns, correlation coefficients were computed between the model computed surface currents and the measured velocity profile throughout the depth. Due to the larger flow variance and the reduced impact of coastal bathymetry, this component of the study focused on data from probe A only (in the outer bay). The objective of the comparison was to gain further insight into the relative importance of the barotropic (vertically unsheared) and baroclinic flows within the domain. Fig. 5 presents the Pearson correlation computed between model computed surface currents and the measured flow at each ADCP bin. The measured velocity profile extends from the surface to a depth of approximately 35m. In both the zonal and meridional components one observes increasing correlation up along the water column; this trend is interrupted in the topmost ADCP bin where correlation drops markedly due to the expected surface reflection contamination. Excluding the topmost bin the average correlation coefficient is 0.66 and 0.51 in the zonal and meridional direction respectively.

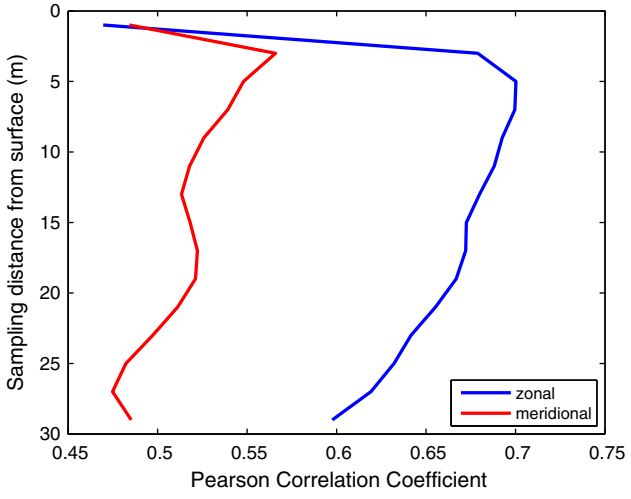


**Fig. 5.** Vertical profile of correlation computed between model computed surface currents and measured velocities throughout the depth. Correlation computed separately in the zonal (blue line) and meridional (red) direction.

In any model-HFR study, the validation of both model and HFR output is fundamental. The performance of both datasets was assessed by direct comparison with ADCP measurements collected near the centre-point of the HFR measurement footprint. The probe was deployed from 29th June to 1st October 2013 and data from the bin nearest the surface with reliable data (5.2m depth), used for the analysis. Fig. 6 presents a time series comparisons of the datasets for selected time window. Results demonstrate close agreement between ADCP and HFR particularly in the zonal direction. Quantifying the differences returns RMSD of 11.9cm/s and 9.7cm/ in the zonal and meridional direction respectively. Meridional RMSD is less primarily due to lower ambient flows. Analysing Fig. 6 shows that there is considerable disagreement in this direction. Computing relative metrics of agreement the zonal direction returns correlation and model skill score of 0.72 and 0.83 respectively, while corresponding values in the meridional direction equated to 0.13 and 0.48. These metrics demonstrate the superior agreement between sensors in the zonal direction. A number of hypothesis are plausible considering this directional discrepancy, including, lower ambient speeds in the meridional causing increased sensor inaccuracies, and highly wind-driven meridional flows inducing more small-scale processes than the predominantly tidally-driven zonal flows. In evaluating these comparisons, it is important to bear in mind the different spatial scales being measured by the two sensors. However, considering the relatively high spatial resolution of this HFR installation (300m grid cells), it seems reasonable to adopt these measurements as an upper bound on HFR uncertainty (Yoshikawa et al., 2006).

Similarly Fig. 6 demonstrates that model results agree well with ADCP measurements. In particular the trend of the flows characterised by semi-diurnal flows is accurately reproduced by the model. The model performs better than the HFR in resolving flows in the meridional direction. However, the model consistently underestimates actual magnitudes of flows in this direction. RMSD metrics return values of 7.69*cm/s* and 5.87*cm/s* in the zonal and meridional direction respectively. The ability of the model to produce the trends of the flows was reflected in high values of linear correlation in both directions (0.9 and 0.54 in the zonal and meridional direction respectively). A relative metric of agreement as provided by the skill score yielded similar values of 0.94 and 0.58 respectively. These metrics suggest that the model performs better than the HFR system in quantifying flows. However, the depth of measurement is a critical consideration in this comparison. As mentioned previously, the depth of measurement of the ADCP is at 5.2m while the HFR samples at approximately 0.5m. It is apparent that wind forcing is more influential nearer the surface. Analysing Fig. 6 suggests that ADCP measured flows are primarily a function of tidal flows while the HFR data contains flows at different time scales. Hence, while the ADCP comparison provides useful insight into relative performance a detailed analysis of model-HFR data requires a consideration of the various dynamical processes driving flow as will be provided in subsequent sections.

ADCP-model comparisons focused primarily on the depth-averaged flows: readings were averaged over the total water depth excluding the uppermost five metres of the water column, and compared with equivalent depth-averaged flows computed by the model. Fig. 7 presents depth-averaged ADCP measured currents plotted against model data at location A for a subset of the study period, while Fig. 8 assesses the performance of the model at location B. Results demonstrate that the model performs well in simulating actual field conditions. Generally good agreement exists between computed and measured flows. Fig. 8 amounts to an RMSD and model skill score of 6.8 *cm/s* and 0.78 respectively, while the datasets presented in Fig. 7 correspond to an RMSD of 8.3 *cm/s* and a skill score of 0.86. Comparable values were computed by Warner et al. (2005) in the Hudson River estuary where skill of 0.68–0.89 were recorded.

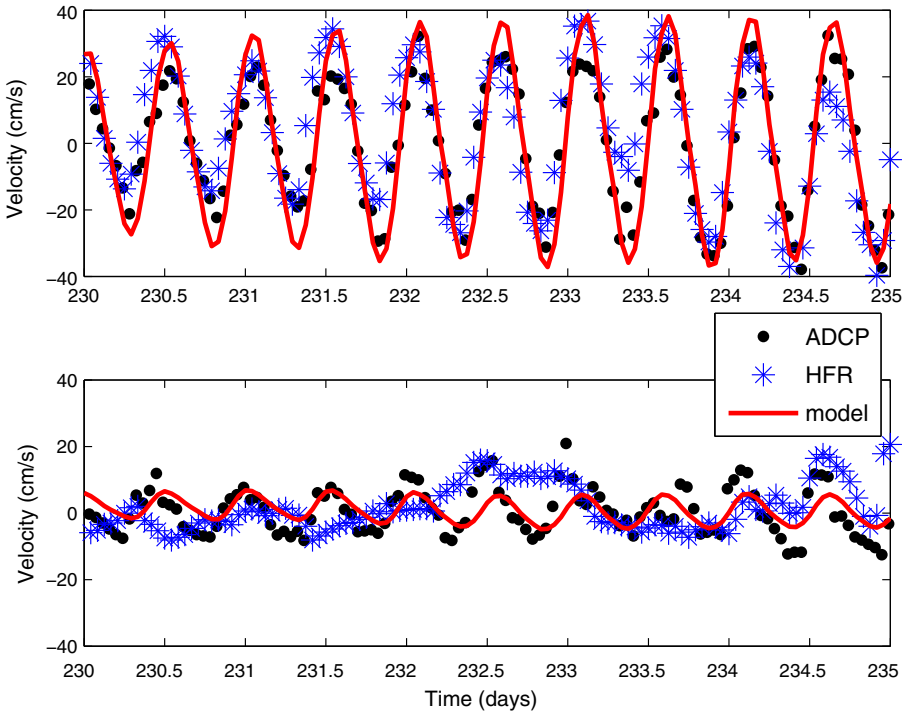


**Fig. 6.** Time series comparisons of the zonal (top) and meridional (bottom) components of surface flows for HFR and ADCP observations compared with model output at location H3 denoted in Fig. 2.

Prior to more detailed comparisons of numerical and HFR data, the ability of the model to replicate observed surface currents at individual points was investigated. Figs. 9 and 10 present time series plots at two distinct regions of the model domain: within the outer bay (Fig. 9), currents are generally greater and flows can reasonably be expected to be dominated by tidal flows; at location H2 secondary forcings such as wind and coastal bathymetry are expected to have a greater influence. Analysing time series data exhibits a number of interesting features. In the zonal direction, model and HFR observations demonstrate appreciable agreement; notwithstanding the higher variability of the measured data, the general trends of flows in the zonal direction are closely replicated by the numerical simulations. In the meridional direction, model performance is diminished considerably. Apart from some instances in time, there is clear mismatch between both data. Model simulations consistently under-estimate observed surface currents, while a temporal phase shift is observed during a portion of the data time window in Fig. 9.

Model-ADCP comparisons provides further insight into these trends. Fig. 7 in the outer bay, demonstrates that the model tends to accurately replicate zonal flows but overestimate meridional peak speeds. Fig. 8 demonstrates inconsistencies in terms of the phase of the tidal cycle. The proximity of land at this location is expected to steer flows in a East-West direction along the shoreline; however ADCP measurements show that while flows are predominantly thus aligned, periods of greater variability are also observed, with a strong North-South flow observed on the dates 15th–16th May. A possible reason for the discrepancy between model and sensor is that the model is not capable of replicating the small-scale flow features that the ADCP is measuring.

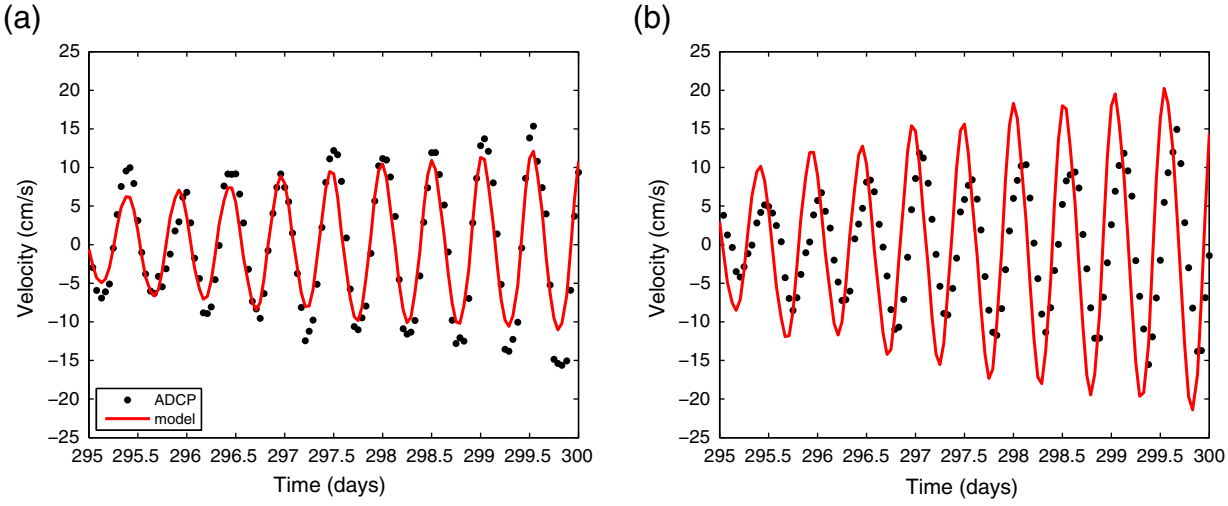


**Fig. 7.** Depth-averaged model computed and ADCP measured (a) zonal and (b) meridional direction current speed time series comparison in the outer bay (location presented as A in Fig. 1).

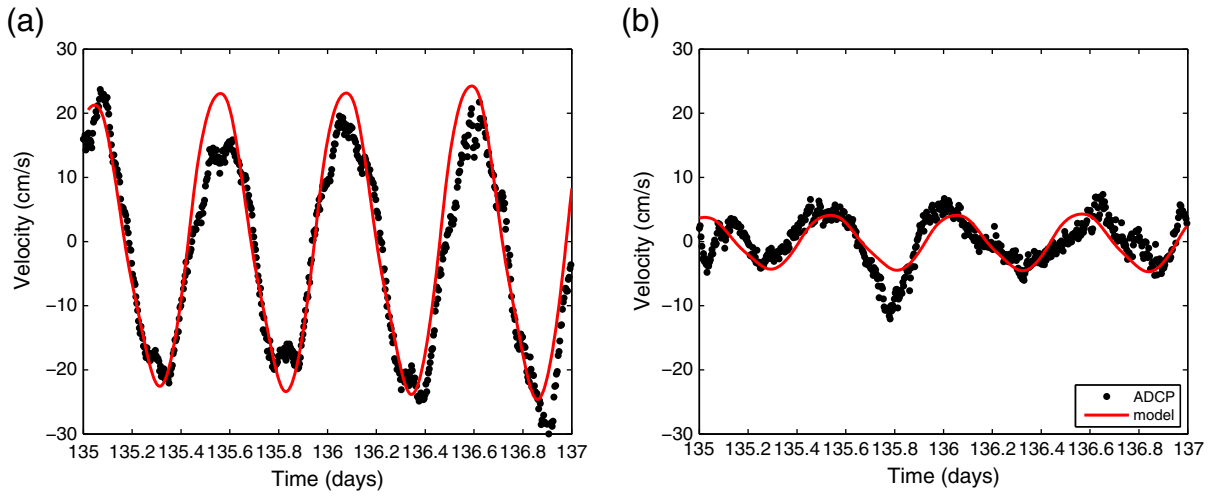


**Fig. 8.** Depth-averaged model computed and ADCP measured (a) zonal and (b) meridional direction current speed time series comparison within the inner bay (location presented as B in Fig. 1).

The discrepancy between the model resolution of 300m horizontal resolution and the ADCP which is essentially a point measurement will be particularly exacerbated at this location where the representation of both bottom bathymetry and coastal bathymetry will be of utmost importance.

To summarise this section Table 1 presents an overview of the field data included in this study along with the measurement period and location.

### 3.2. Flow-field analysis

As a measure of the mean deviation of model output from HFR observations, Fig. 11 presents the RSMD between simulated and measured flows for the month of December 2011. Mean RMSD across the bay equalled 23.8$cm/s$ with isolated area of higher RMSD at the outer extents of the measurement footprint, and along the baseline of the radar sites. Comparisons with ADCP discussed in the previous section estimates HFR uncertainty for this study site between $10 - 12cm/s$. Considering both the computed HFR uncertainty and the reported RMSD between model and observations, these results suggest model uncertainties of $12 - 14cm/s$. Regions of higher reported RMSD require further consideration, however.

Along the baseline, the accuracy of the radar is conceivably lower due to GDOP issues. Near the baseline, total vectors are not accurate because the radial velocities are nearly parallel (Barrick, 2006). To further investigate the expected amplification of uncertainty within this region, Fig. 12 presents Pearson's correlation coefficient between model and HFR. In conjunction with this, model skill scores were computed (Fig. 13), to better quantify localised discrepancies allowing for ambient flow speeds, and in particular lower flows in the baseline region along the Northern shore. In this region, ambient flow speeds are lower than in other areas of the bay and RMSD may provide a potentially misleading representation of the true deviation which may be better quantified by the above metrics. Both metrics are presented decomposed into the zonal and meridional component of flow. Along the baseline, the meridional component of flow is distorted most by GDOP, while the zonal component is accurately resolved, apart from a very small region along the shoreline due to a slight rotation of the baseline from East-West. Analysing, Figs. 12b and 13b suggests that GDOP is not having a significant impact on results in this study. There is no evident drop in agreement between meridional datasets along this narrow region. While there is a slight increase in RMSD along the baseline, the actual uncertainty intrinsic in the HFR itself rather than any introduced by geometric issues seem dominant. (Barrick, 2006) introduced an expression for computing GDOP based on the placement of a pair of HF radar sites.

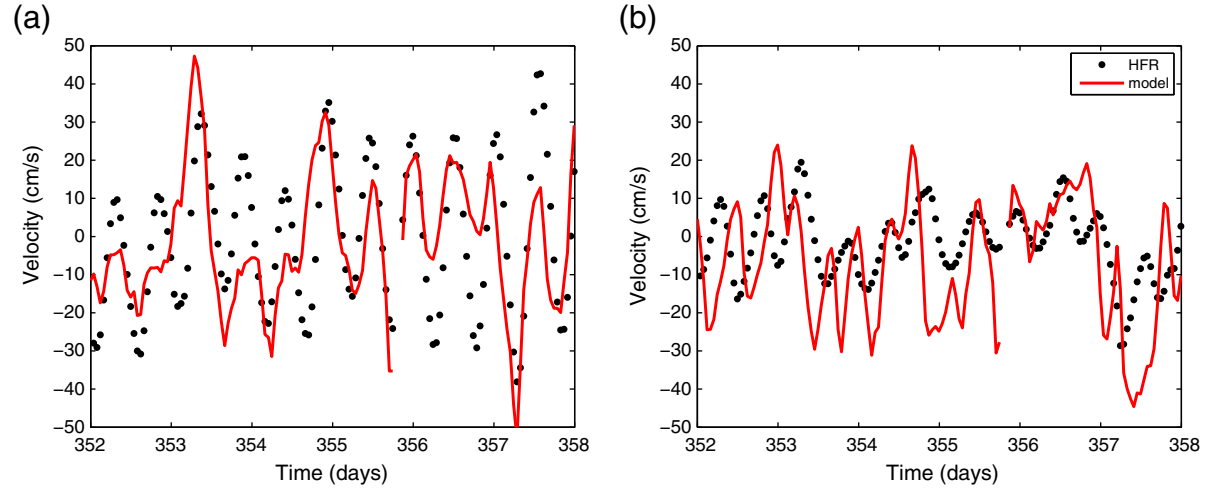


**Fig. 9.** Time series comparison of the (a) zonal and (b) meridional components of surface flows for HFR observations and model simulations at location H1 denoted in Fig. 2.

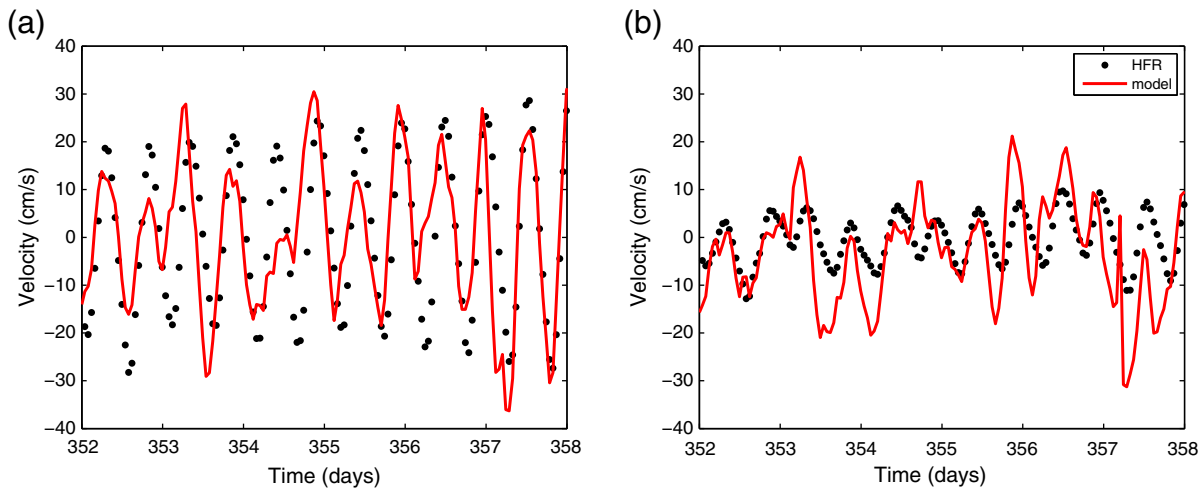


**Fig. 10.** Time series comparison of the (a) zonal and (b) meridional components of surface flows for HFR observations and model simulations at location H2 denoted in Fig. 2.

Applied to this study site, GDOP uncertainty amplification drops below 2 south of latitude 53.22° (not presented). The localised region of high RMSD denoted in Fig. 11 extends significantly further than this suggesting factors other than GDOP are dominant in the reported deviations.

A notable discrepancy exits between the insight provided by the different metrics of agreement. The magnitudes of correlation returned in both the zonal and meridional are noticeably less than model skill for the equivalent flows, if one considers both to range from 0 (no agreement) to 1 (perfect agreement). In the zonal direction, mean model skill equals 0.7 while correlation is less than 0.5 over much of the bay. A similar trend was observed earlier when comparing meridional flow measurements from HFR and ADCP. Quantifying differences returned relatively high skill agreement (0.48) compared to correlation (0.13) for the same datasets. A visual comparison of Fig. 6 suggests that there is some agreement between the two datasets with the actual magnitudes of deviations often quite low. This aspect however will not be reflected by linear correlation techniques. This highlights the complexity inherent in assessing agreement between synoptic datasets susceptible to small-scale variability in space and time. Pearson's correlation coefficient describes consistent linear increases or decreases about the respective means of the two variates; however, it makes few distinctions between the type or magnitudes of possible covariations. The model skill score proposed by Willmott (1981) circumvents some of these problems by instead computing the degree to which the observed variable is accurately estimated by the model. However, a potential source of uncertainty in the model skill score (and other similar indices of agreement) is that it fundamentally compares predicted and observed variability about the mean of the observation ($\bar{O}$), as $\bar{O}$ is often the best available estimate of the true average. Sampling and other representational problems, however, may render $\bar{O}$ a suboptimal representation of central tendency in some circumstances. A better estimate of the true mean for instance may be one that varies over space and time rather than one that is averaged over the entire domain (Willmott et al., 2012). This reflects in that a single metric of agreement does not quantify model performance in all cases and as advised by Willmott (1981), a number of metrics should be presented with at least one absolute and one relative.

Further analysing the presented metrics on model skill indicates a distinct discrepancy in the zonal and meridional measures of agreement. Model skill in the zonal direction corresponds to a mean value of 0.7 across the bay while in the meridional direction this value reduces to 0.56. A possible reason for this is the different forcings, primarily tides and winds, driving flows within the bay, and the skill of the model in simulating these forcings. In the central region of the bay, tidal flows are predominantly zonal (Booth, 1975). This is reflected in the ADCP measured flows presented in Fig. 8 where the zonal flows are up to a factor of four greater than meridional flows. Wind forcing in the bay, however, is predominantly south-westerly (Fig. 3). This suggests that the more linear, tidal forcing component is both well resolved by the model and measured by the HFR. Wind forcing, however, is expected to be more variant in time and space, while there exists a non-linear relationship between wind and resultant currents (Smith, 1988). It is reasonable that resolving wind-driven surface currents in a model poses inherent difficulties, while, the space and time averaging procedures adopted by the HFR to produce hourly current maps eliminates information on horizontal shear and variations in the current velocity field over time. It is the objective of the remainder of this study to better understand the fundamental nature of these issues and attempt to use both datasets and their inherent uncertainties to better describe the actual flow structure.

**Table 1**
Summary of sensor location, measurement period and data inter-comparisons conducted as part of this study.

| Comparisons | Location | Time Period | RMSD |
|---|---|---|---|
| Model – Tide gauge | − 9.05°W, 53.27°N | Continuous | - |
| Model – ADCP | A (− 9.47°W, 53.08°N) | 26/09–14/11/2011 | 6.8 |
| Model – ADCP | B (− 9.26°W, 53.23°N) | 01/05–13/05/2007 | 8.3 |
| Model – ADCP | C (− 9.15°W, 53.2°N) | 29/07–01/10/2013 | 6.6 |
| ADCP – HFR | C (− 9.15°W, 53.2°N) | 29/07–01/10/2013 | 9.8 |
| Model – HFR | Spatial domain | 01/12–31/12/2011 | Fig. 11 |

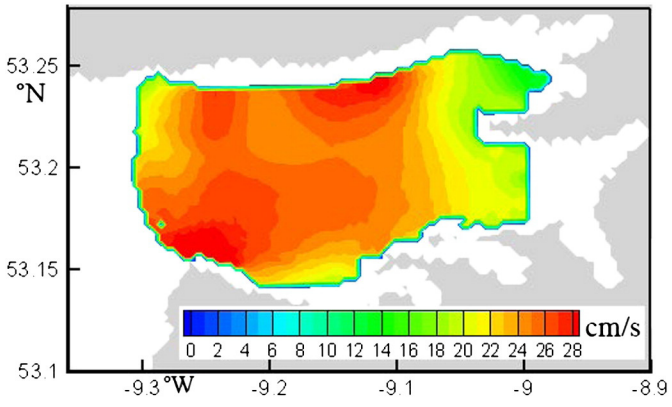


**Fig. 11.** RMSD between model simulations and HFR observations for the month of December 2011. Magnitudes of deviations denoted in colour bar.

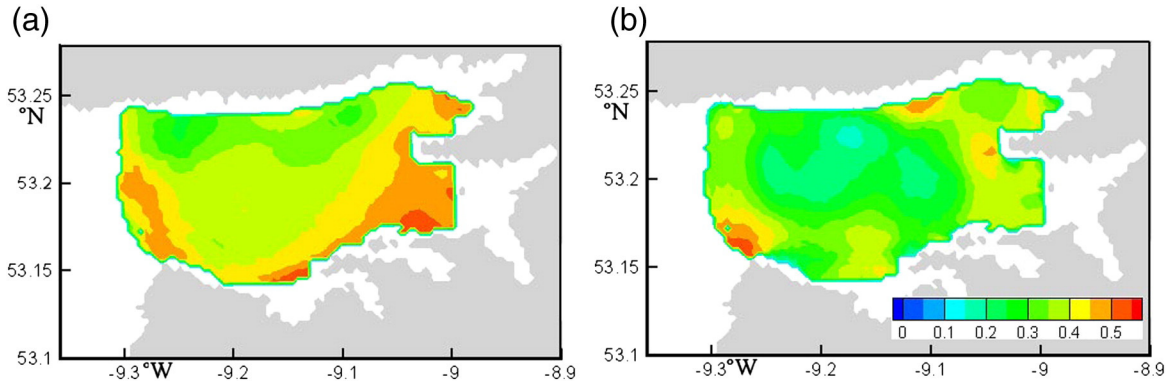


**Fig. 12.** Pearson's linear dependence correlation coefficient between model computed and HFR measured surface currents in the (a) zonal and (b) meridional direction for the month of December 2011.

### 3.3. Tidal analysis

Tidal currents are considered one of the more robust observations made by HF radar systems (Paduan and Washburn, 2013) and can be considered a verifiable dataset to assess fundamental model physics. As with the rest of Irish coastal waters, the semi-diurnal tide dominates in Galway Bay with mean spring and neap tidal range in the bay of 4.9m and 1.79m respectively.

This component of flow in both observational and numerical datasets was investigated via a two-pronged approach. Initially, the ability of the model to simulate tidal flows was assessed by comparison with the tidal component only of the HFR data. Secondly tidal ellipses of the dominant tidal constituent were computed and plotted to provide a singular pictorial representation of primary flows within the bay (May, 1979).

Numerical simulations incorporating tidal forcing only (excluding both wind and density-driven flows), constituted the baseline run for assessing the fundamental performance of the numerical model hydrodynamics. In conjunction with this, the HFR data were processed via the t_tide software, a set of Matlab programs for performing harmonic analysis of oceanic tides (Pawlowicz et al., 2002). Finally, $|\rho|$, the magnitude of complex correlation coefficient was computed, between the harmonic component of the HFR data, and output from the barotropic model simulations. Fig. 14 shows the magnitude of complex correlation between the data pairs.

Analysing Fig. 14 suggests the model adequately simulates tidal dynamics within the bay. Mean correlation averaged across the bay equals 0.53 with a standard deviation of 0.13. Considering the high level of activity present within the surface layer, this can be considered an acceptable degree of correlation and is similar to measures of correlation observed in comparable studies (Lewis et al., 1998).

Tidal analysis enables the representation of the time series of vector surface currents in terms of ellipse parameters. Given the orthogonal velocities $u$ and $v$ which are periodic with some frequency $\omega$, the complex vector $u + iv$ can be formed. This vector may be decomposed into two constant, complex vectors rotating in opposite directions. These rotating vectors alternately add to, or subtract from one another producing the characteristic shape of the tidal ellipse. The phase of the vectors determine which direction the ellipse is orientated (May, 1979). The resultant data permit convenient representation as tidal ellipses for each constituent.

Fig. 15 presents tidal ellipses calculated from HFR and model data. For comparisons, data from two model simulations are presented: Fig. 15(b) presents model output with barotropic flows only driving the model (i.e. tide and wind) while Fig. 15(c) presents model results with full barotropic and density-driven baroclinic forcing (hereafter termed full baroclinic model). For a more equitable comparison, wind forcing was included in both model simulations Analysing plots of both observational and numerical ellipses yields similar trends for both datasets, particularly in the zonal direction where the semi-major axes are of similar magnitudes. Averaged over the entire domain the absolute difference between observations and modelled semi-major axis are 4.79 *cm/s* for barotropic simulations and 4.99 *cm/s* for full baroclinic simulation; while, the deviations along the semi-minor axis equal 0.8 *cm/s* and 0.3 *cm/s* respectively. Results demonstrate considerable variance spatially. In the outer extents of the bay where tidal activity is greatest, observations demonstrate a clear meridional component of flow. This is approximated somewhat by the full baroclinic simulation but not by the barotropic model which computes a semi-minor axis approaching zero. Quantifying the outer bay dynamics, mean absolute differences in semi-major axis equals 3.42*cm/s* and 2.35*cm/s* while semi-minor axis differences are 3.61*cm/s* and 1.79*cm/s*, for barotropic

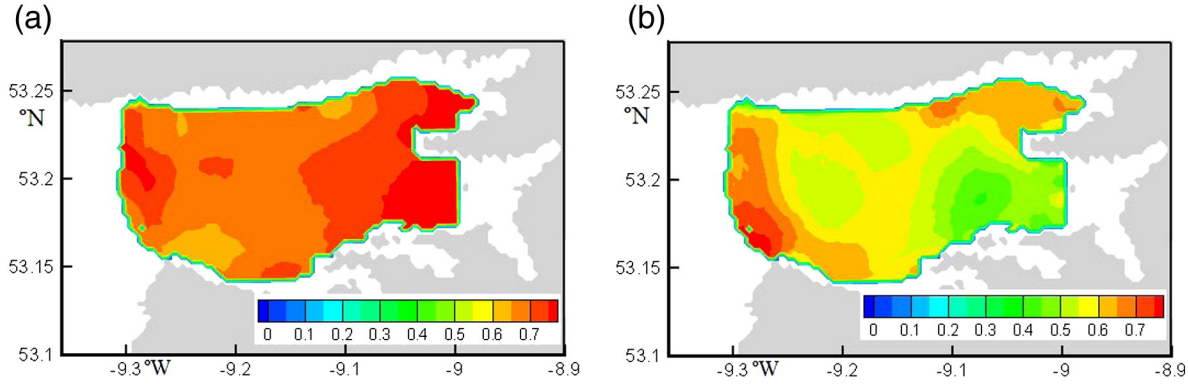


**Fig. 13.** Model skill score for the (a) zonal and (b) meridional velocity component.

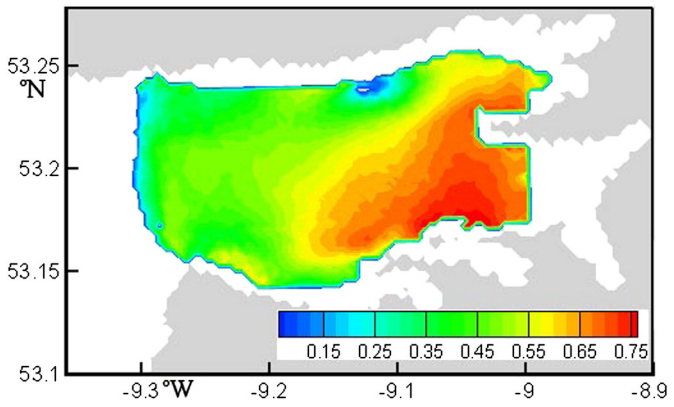


**Fig. 14.** Complex correlation coefficient $|\rho|$ computed between EFDC driven by tidal forcing only and the tidal component of HFR observations.

and full baroclinic simulations, respectively. Across the domain as a whole the barotropic model outputs lower ellipticity (ratio of semi-minor axis to semi-major) than both the full baroclinic model and in particular observations. This implies that baroclinic flows plays an important role in dynamics within the bay. Interestingly the orientation of the ellipses is similar in both plots suggesting the model is replicating some of the general trends of the flows, but not the more complex circulatory patterns described by the ellipticity. Again, analysing absolute differences of orientation across the bay versus observations yields values of 32.2 ° and 24.2 ° for barotropic and full baroclinic simulations respectively. Similar results were observed by Mau et al. (2007) who investigated barotropic flows in the New York Bight by combination of HF radar and numerical simulations. In that study model HFR deviations averaged across the domain were 10.8 *cm/s* for semi-major axis and 4 *cm/s* for semi-minor axis, while the misfit in orientation amounted to 29°.

Within the inner bay, ellipses for both HFR and numerical model are predominantly in the zonal direction with ellipticity reducing to almost zero in many cells. This is likely to be a result of the local coastal bathymetry. As currents enter the inner bay, the pronounced ellipticity described previously degenerates rapidly, while the vector orientation is also greatly amended. The resultant forcing is a dominant zonal component aligned with the direction of the coastline. At the inner extents of the bay the alignment with coastal bathymetry is clearly evident with little meridional component of the tidal forcing evident. Tidal ellipses summarize the principal properties of the oscillatory flow (Carbajal and Pohlmann, 2004). Therefore, reproducing satisfactorily ellipses by the numerical model indicates that the model correctly resolves tidal flows. This is particularly true in the near-coast region where studies have demonstrated the difficulties in reproducing observed tidal ellipse properties (Davies et al., 2001).

### 3.4. Wind analysis

In addition to tides, winds are expected to be the other dominant factor driving flows across the bay, with freshwater influences mainly

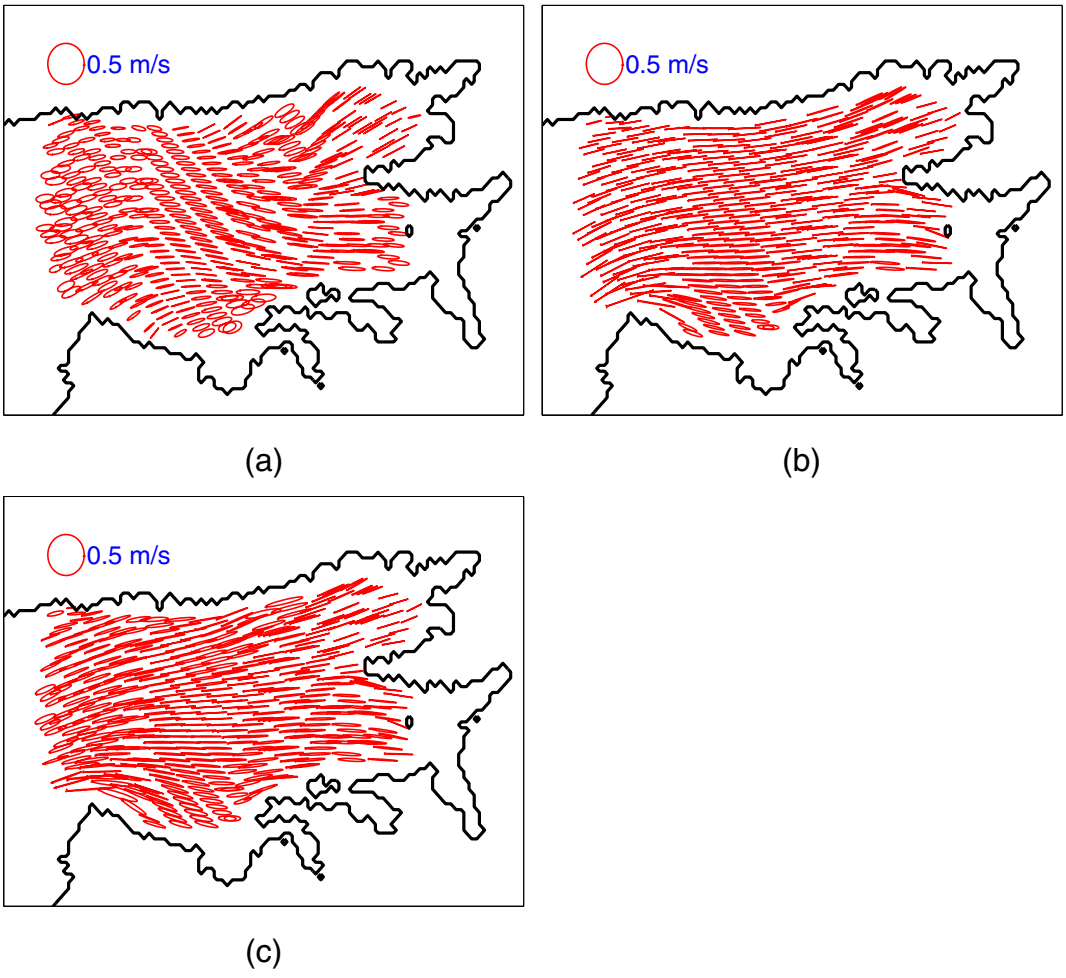


**Fig. 15.** Dominant M2 tidal ellipses derived from (a) HFR observations, (b) barotropic model simulations and (c) barotropic and baroclinic model simulations. Analysis based on one month of data at intervals of 60 minutes (744 samples in time for grid points with full HFR coverage over time).

restricted to the Northern Shore (Booth, 1975). Subtracting the tidal signal computed above from the total flows gives an estimate of the influences of winds on flows (neglecting contribution of density driven flows). As a preliminary analysis the relative contribution of both components for the HFR and model data was computed. The kinetic energy per unit volume was computed as $\frac{1}{2}\rho\overrightarrow{U}^2$ for the tidal and residual component of the dataset. As might be expected the total kinetic energy of the HFR dataset was higher suggesting again that a considerable portion of the total variance of the system was not being captured by the model. The mean kinetic energy of the tidal component of the HFR system amounted to $5.07 \times 10^4$ Joules with the residual component having a mean kinetic energy of $9.73 \times 10^4$ Joules. Model data on the other hand contained tidally driven mean kinetic energy of $7.04 \times 10^4$ Joules with the residual component accounting for $3.7 \times 10^4$ Joules.

These results suggests that the model is not adequately capturing the magnitudes of wind driven flows within the bay. To further investigate the performance of the model in capturing qualitative aspects of these flow processes, complex correlation coefficient of surface currents with HIRLAM winds were computed. Correlation was computed separately for both total and non-tidal, residual currents based on both HFR observations and numerical model results. Fig. 16 presents the magnitude of correlation for the computed values.

Analysing Fig. 16 yields a number of interesting features. Chief amongst these is a marked drop in correlation between numerically computed surface currents and wind in the central region of the bay. A similar trend, although not as pronounced, is evident within HFR data, with correlation for both highest at the outer extents of the domain. A possible cause for this is the complex flow dynamics known to develop within the inner bay characterised by circulatory flow patterns and strong non-persistent gyre formations (Booth, 1975). Gyres have been shown to develop during periods of large tidal motion and light wind conditions (Ragnoli et al., 2012), with tidal action resulting in the gyre structure being transported about the bay with the bulk advection of tidal motion. This study demonstrates that barotropic flows are well predicted by the model with strong correlation between depth-averaged model and ADCP observations reported. However, analysis of Fig. 16 suggests that tidal flows are a combination of barotropic and baroclinic flows with better agreement between measured and modelled tidal ellipses observed when baroclinic flows also included (Fig. 15c). In conjunction with the apparently low correlation observed in this study, this infers that residual surface currents are not a simple function of a single forcing (i.e. wind); rather, these results suggest that surface currents within the inner region of the bay are a complex combination of wind forcing, tidal actions and local topographical effects. A detailed study of surface current response to wind forcing involves three primary consideration: nonlinear temporal relationships, the spatial decorrelation of surface currents and wind speeds, and reported anisotropic current response due to coastal topography and anisotropic bottom drag (Kim et al., 2009). The linear relationship proposed here has potential to provide some insight into wind effects on surface currents, and in particular identify local shortcomings. However, a detailed analysis requires the inclusion of the various dynamical processes of air-sea interaction and extend beyond the scope of this study. These issues are discussed in further details in the next section.

## 4. Discussion and conclusions

The objective of this research is an investigation of circulation patterns within a bay by combining ADCP, HFR measured data and model simulations; in particular, an assessment of the main mechanisms driving surface flows, and the ability of these different methods to capture flow processes. ADCP comparisons permit an independent assessment of the performance of both HFR and model in resolving complex surface currents. This analysis reports an RMSD of 9.8*cm/s* and 6.6*cm/s* for HFR and model respectively. In both these metrics important measuring differences exist, in particular, the different spatial scales sampled by the ADCP as opposed to the HFR or model grid resolution. The HFR set-up dictated a grid size of 300m while the model was constrained primarily by computational cost to an equivalent grid size.

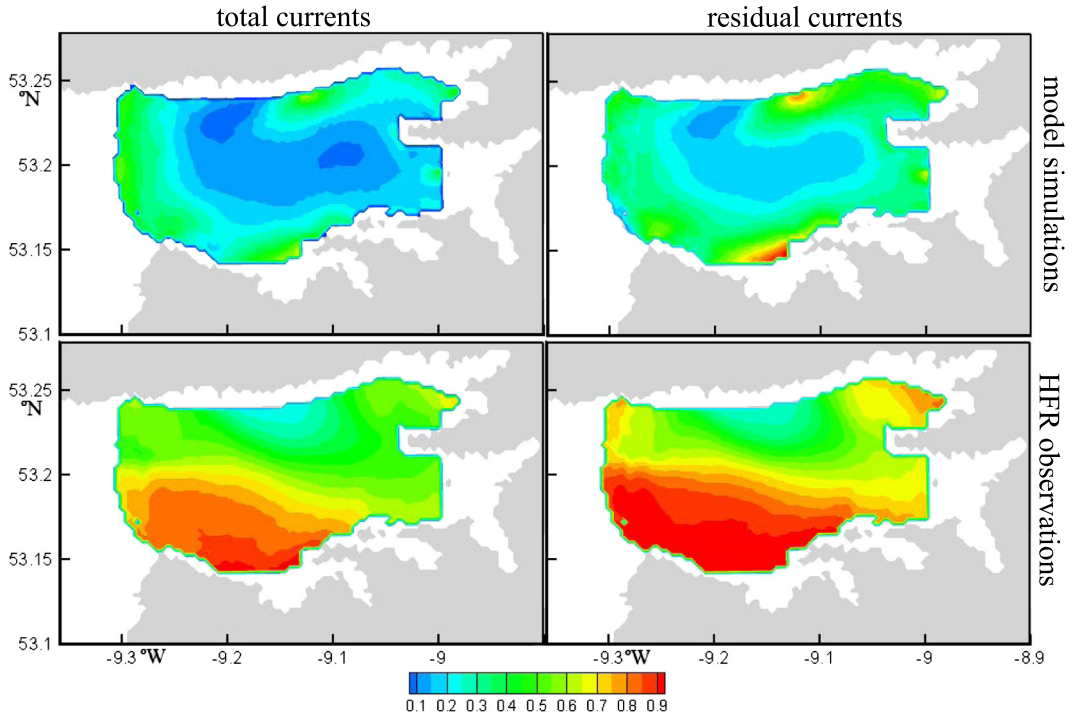


**Fig. 16.** Magnitude of complex correlation $|\rho|$. between model simulations (top row) and HFR observations (bottom row). The left hand side presents correlation between wind and total surface currents, while on the right is correlation when the tidal component of flow removed by harmonic analysis. Correlations computed versus HIRLAM wind information. Study period encompasses a 31 day period in December 2011, leading to a maximum number of samples per grid point of 744.

This is likely to impact on the ability of both the HFR and model to resolve the smaller scale flow features sampled by the ADCP. To investigate this further, current studies are focusing on high resolution studies of the bay permitted by an MPI parallel version of the EFDC model recently implemented by the authors (O'Donncha et al., 2014). In addition, the depth of measurement of the ADCP potentially reduces sensitivity of the flow to wind forcing as opposed to the near-surface HFR measurements. Due to surface contamination of the upper bins ADCP data is from a measuring depth of 5.2$m$. Hence, care is needed when adopting the ADCP data to quantify uncertainty in both the model and HFR. Instead, following the work of Yoshikawa et al. (2006), these RMSD values can be adopted as an upper bound on system uncertainty.

Direct comparisons between HFR and numerical model data provide further insight into the accuracy of each in resolving surface current dynamics. Typical RMSD across the bay lies in the range $14 - 24cm/s$ as discussed in Section 3.2. These are of similar magnitude to values computed by (Port et al., 2011) in model/HFR comparisons conducted in the German Bight and larger than the values of $5 - 15cm/s$ observed by Kaplan et al. (2005) when comparing ADCP and HFR observations in the Bodega Bay region. A study by (Emery et al., 2004) comparing HFR and moored current meters in the Santa Barbara basin indicated rms differences of $7 - 19cm/s$. In a similar study by (Essen et al., 2000), the accuracy of HFR was assessed by comparison with in situ current meters. RMSD were in the range of $10 - 20cm/s$, however, the theoretical uncertainty of the HFR based on the sea state was estimated to only be in the range $3 - 10cm/s$. The rest was assumed to be due to the differences of the quantities measured, e.g. the spatial averaging, point in water column at which measurement recorded. Yoshikawa et al. (2006) estimated the uncertainty within an HFR system by comparisons with ADCP measurements and also by baseline comparisons between facing HFR sites. Comparisons with ADCP yielded RMSD in the range $6.62 - 11.3cm/s$ while baseline comparisons, termed a lower bound on HFR uncertainty, returned RMSD of $5.75 - 13.3cm/s$. In this study, direct comparisons with ADCP, presented in Section 3.1, suggests HFR uncertainties in the range of $10cm/s$, while ADCP RMSD was in the range $6.8 - 8.3cm/s$. Assuming that uncertainty from both model and HFR contributes to the total RMSD then these values broadly coincide with the computed model-HFR RMSD presented in Fig. 11. The results of these analyses enable an estimate of uncertainty distributed between sensor measurement and model output; this serves as a foundation for the more detailed investigation of distinct flow processes.

Skill score analysis of HFR/model output highlight the distinct discrepancy between results in the meridional direction. Further investigation suggest this to be a failure of the model and HFR to adequately capture wind-driven flows. ADCP comparisons demonstrate that the model accurately replicates depth-averaged flows. Complex correlation statistics and tidal ellipses support this evaluation: spatial correlation coefficients between the tidal component of the HFR signal and barotropic model simulations show acceptable levels of agreement as shown in Fig. 14 and discussed in Section 3.3. Complex correlation magnitudes of 0.6–0.8 computed in the inner bay reduce to values of circa 0.4 moving away from the radar site suggesting a logical relationship between accuracy of HFR observations and distance from radar sites; HFR fundamental operational theory informs that measurement confidence decreases moving away from the radar site due to the larger horizontal averaging area of the radial cell (Lipa, 2003). Plots of tidal ellipses displays quite similar trends between HFR and numerical datasets. In both cases a strong zonal component of currents is apparent while the orientation of the ellipses are generally quite similar.

As mentioned, discrepancies exist between the computed ellipticity of both datasets. This is particularly pronounced in comparisons between model simulations incorporating barotropic tides only where ellipticity reduces to zero across much of the bay. The results imply that baroclinic flows are an important forcing mechanism in the bay. This is particularly evident along the Northern shore where the ellipticity observed from HFR is simulated to a much greater degree when baroclinic forcing are also included (Fig. 15c); in this region freshwater interaction are at their most significant as the bulk inflow from the River Corrib traverses along the Northern shoreline exiting the bay through the North Sound (Nolan, 1997). Analysis of correlation coefficients computed between model and ADCP (Fig. 5) further demonstrate the importance of baroclinic shears. The vertical profile of correlation between model surface currents and measured vertical velocity profile illustrates a continuous increase in agreement along the water column (ignoring the ADCP surface layer which can suffer data contamination). If hydrodynamics in the bay consisted of barotropic tides only one would expect similar correlation at all depths; instead, these results demonstrate that a density induced gradient exists in the vertical profile of horizontal flows.

While adequately replicating tidal dynamics, decomposition of wind driven components of flows highlight a number of issues. Separate analysis on zonal and meridional components display low correlation magnitudes along the direction of prevailing winds; while statistical analysis of decomposed model surface current residuals display low correlation with winds. These results suggest a low sensitivity of the model to wind stresses with tidal and baroclinic forcing dominating. A number of hypotheses explaining this discrepancy are possible, namely: discrepancies between regional-scale, coastal-ocean models and bay-scale dynamics which are a product of both local and global scale effects (Song and Haidvogel, 1994); model errors arising from highly-variable wind-driven flows across a large body of water forced by point measurements of wind speeds and direction; and the high dependence of model simulations on empirical wind-stress coefficients.

Common practise in ocean modelling is the adoption of a sparsely distributed number of, often land-based, wind speed measurements to parameterise wind stress in simulations. These datasets are often averaged to provide a singular measure of wind speed across the model domain. The assumption that wind-speed is constant across the bay is often questionable with superior results obtained when using high resolution vector wind forcing (Chao et al., 2003). Wind stress in ocean models is parameterised in terms of wind density, wind speed and the interfacial drag coefficient. While wind speed and density are relatively easily quantified, the parameterisation of drag coefficient is more complex (Taylor and Yelland, 2001).

Typical formulations involve a linear or polynomial dependence on wind-speed. The EFDC model adopts the following formula for calculating wind stress:

$$\tau_x = 1.2 \times 10^{-4}(0.8 + 0.065U)U.u \tag{5}$$

where $\tau_x$ is wind stress in $x$ direction ($N/m^2$),while $U$ and $u$ represent surface layer current speed and 10m wind speed in x direction respectively. Different formulations can be implemented and impact the accuracy of the instantaneous and long-term residual circulation. Investigating different parameterisations, Bonekamp et al. (2002) found that a sea-state dependent Charnock parameter was marginally superior. While current speed, available at each model timestep, can easily be incorporated, the inclusion of wave speed is problematic and currently limited to a statistical treatment (Kara et al., 2007). Further, recent studies by Brown et al. (2013) suggested that application to coastal sites required case-specific tuning with the coefficient dependent on both model resolution and local bathymetry. These factors highlight the difficulty in accurately simulating wind forcing in ocean model simulations, particularly in coastal regions where topographical steering further impacts on flows. Results presented in this research highlight areas where improvements of the numerical model could be focused. Central to these is to use the comprehensive verification potential presented by HFR datasets to derive superior wind stress formulation or to use the real-time surface current measurements to improve the model by assimilation methods. However, as this study demonstrates, this is not a trivial matter with any

implementation demanding a stringent consideration of measurement uncertainties and inaccuracies prior to assimilation into a model.

## Acknowledgements

Elements of the research were supported by the EnergyMARE and MAREN2 projects which are part-funded by the European Regional Development Fund (ERDF) through the Atlantic Area Transnational Programme (INTERREG IV).

## References

Bai, S., Lung, W., 2005. Modeling sediment impact on the transport of fecal bacteria. Water Res. 39 (20), 5232–5240.
Barrick, D., 2006. Geometrical dilution of statistical accuracy (GDOSA) in multi-static HF radar networks. Technical report; Codar Ocean Sensors Report.
Barrick, D.E., Evans, M.W., Weber, B.L., 1977. Ocean surface currents mapped by radar. Science 198, 138–144.
BIM, 2012. Environmental impact statement for deep sea fish farm development in Galway Bay. Technical report. Irish Sea Fisheries Board.
Bonekamp, H., Komen, G., Sterl, A., Janssen, P., Taylor, P., Yelland, M., 2002. Statistical comparisons of observed and ecmwf modeled open ocean surface drag. J. Phys. Oceanogr. 32 (3), 1010–1027.
Booth, D., 1975. The water structure and circulation of Killary Harbour and of Galway Bay(Ph.D. thesis) Department of Oceanography, National University of Ireland, Galway.
Breaker, L.C., Rao, D.B., Kelley, J.G., Rivin, I., 2004. Development of a real-time regional ocean forecast system with application to a domain off the U.S. east coast. Mar. Technol. Soc. J. 38 (1), 61–79.
Brink, K.H., 1991. Coastal-trapped waves and wind-driven currents over the continental shelf. Annu. Rev. Fluid Mech. 23, 389–412.
Brown, J., Amoudry, L., Mercier, F., Souza, A., 2013. Intercomparison of the charnock and coare bulk wind stress formulations for coastal ocean modelling. Ocean Sci. 9 (4), 721–729.
Bryan, K., Cox, M.D., 1968. A nonlinear model of an ocean driven by wind and differential heating: Part I. Description of the three-dimensional velocity and density fields. J. Atmos. Sci. 25, 945–967.
Carbajal, N., Pohlmann, T., 2004. Comparison between measured and calculated tidal ellipses in the german bight. Ocean Dyn. 54 (5), 520–530.
Chao, Y., Li, Z., Kindle, J., Paduan, J., Chavez, F., 2003. A high-resolution surface vector wind product for coastal oceans: Blending satellite scatterometer measurements with regional mesoscale atmospheric model simulations. Geophys. Res. Lett. 30 (1), 1013.
Chapman, R.D., Shay, L.K., Graber, H.C., Edson, J.B., Karachintsev, A., Trump, C.L., Ross, D.B., 1997. On the accuracy of HF radar surface current measurements: Intercomparisons with ship-based sensors. J. Geophys. Res. 102 (C8), 18,737–18,748.
Davies, A., Jones, J., 1992. A three-dimensional wind driven circulation model of the Celtic and Irish Seas. Cont. Shelf Res. 12 (1), 159–188.
Davies, A.M., Hall, P., Howart, M., Knight, P., Player, R., 2001. Comparison of observed (HF Radar and ADCP measurements) and computed tides in the north channel of the irish sea. J. Phys. Oceanogr. 31, 1764–1784.
Egbert, G., Erofeeva, S., 2002. Efficient inverse modeling of barotropic ocean tides. J. Atmos. Ocean. Technol. 19 (2), 183–204.
Ekman, V., 1905. On the influence of the earth's rotation on ocean currents. Ark. Mat. Astron. Fys. 2, 1–53.
Emery, W.J., Thomson, R.E., 2001. Data analysis methods in physical oceanography. Elsevier Science.
Emery, B.M., Washburn, L., Harlan, J.A., 2004. Evaluating radial current measurements from CODAR high-frequency radars with moored current meters. J. Atmos. Ocean. Technol. 21, 1259–1271.
Essen, H.H., 1994. On the capability of an upward-looking ADCP deployed in the Iceland-Faeroe Frontal Area. Dtsch. Hydrografische Z. 46 (3), 211–228.
Essen, H.H., Gurgel, K., Schlick, T., 2000. On the accuracy of current measurements by means of HF radar. IEEE J. Ocean. Eng. 25 (4), 472–480.
Fernandes, L., 1988. A study of the oceanography of Galway Bay, mid-western coastal waters (Galway Bay to Tralee Bay), Shannon Estuary and the River Shannon plume (Ph.D. thesis) Department of Oceanography, National University of Ireland, Galway.
Galperin, B., Kantha, L., Hassid, S., 1988. A quasi-equilibrium turbulent energy model for geophysical flows. J. Atmos. Sci. 45 (1), 55–62.
Gurgel, K.W., Antonischki, G., Schlick, T., 1997. A comparison of surface current fields derived by beam forming and direction finding techniques as applied by the HF radar WERA. Remote sensing – a scientific vision for sustainable development. IEEE volume 4, pp. 1805–1807.
Hamrick, J., 1992a. A three-dimensional environmental fluid dynamics computer code: Theoretical and computational aspects. Technical report. Virginia Institute of Marine Science.
Hamrick, J.M., 1992b. Estuarine environmental impact assessment using a three-dimensional circulation and transport model. 2nd International Conference on Estuarine and Coastal Modeling. American Society of Civil Engineers, New York, pp. 292–303.
Hamrick, J.M., 1996. User's manual for the environmental fluid dynamics computer code. Technical report. Virginia Institute of Marine Science.
Institute M., 1999. Ireland's marine and coastal areas and adjacent seas: An environmental assessment. Technical report. Marine Institute Ireland.
Ji, Z., 2008. Hydrodynamics and water quality: Modeling rivers, lakes, and estuaries. John Wiley & Sons.
Ji, Z.G., Morton, M.R., Hamrick, J.M., 2001. Wetting and drying simulation of estuarine processes. Estuar. Coast. Shelf Sci. 53, 683–700.
Kaplan, D.M., Largier, J., Botsford, L.W., 2005. HF radar observations of surface circulation off Bodega Bay (northern California, USA). J. Geophys. Res. 110 (25 PP.).
Kara, A., Metzger, E., Bourassa, M., 2007. Ocean current and wave effects on wind stress drag coefficient over the global ocean. Geophys. Res. Lett. 34 (1) L01604.
Khangaonkar, T., Zhaoqing, Y., Degasperi, C., Marshall, K., 2005. Modeling hydrothermal response of a reservoir to modifications at a high-head dam. Water Int. 30 (3), 378–388.
Kim, S.Y., Cornuelle, B.D., Terrill, E.J., 2009. Anisotropic response of surface currents to the wind in a coastal region. J. Phys. Oceanogr. 39 (6), 1512–1533.
Kim, S.Y., Terrill, E.J., Cornuelle, B.D., Jones, B., Washburn, L., Moline, M.A., Paduan, J.D., Garfield, N., Largier, J.L., Crawford, G., et al., 2011. Mapping the US West Coast surface circulation: A multiyear analysis of high-frequency radar observations. J. Geophys. Res. 116 (C3).
Kohut, J.T., Roarty, H.J., Glenn, S.M., 2006. Characterizing observed environmental variability with HF radar surface current mappers and acoustic Doppler current profilers: Environmental variability in the coastal ocean. IEEE J. Ocean. Eng. 31 (4), 876–884.
Kohut, J., Roarty, H., Licthenwalner, S., Glenn, S., Barrick, D., Lipa, B., Allen, A., 2008. Surface current and wave validation of a nested regional HF radar network in the Mid-Atlantic bight. IEEE/OES 9th Working Conference on Current Measurement Technology, pp. 203–207 (CMTC 2008. IEEE; 2008).
Kosro, P.M., 2003. Enhanced southward flow over the oregon shelf in 2002: A conduit for subarctic water. Geophys. Res. Lett. 30 (15), 8023.
Kundu, P., 1976. Ekman veering observed near the ocean bottom. J. Phys. Oceanogr. 6, 238–242.
Legates, D.R., Davis, R.E., 1997. The continuing search for an anthropogenic climate change signal: Limitations of correlation-based approaches. Geophys. Res. Lett. 24 (18), 2319–2322.
Legates, D.R., McCabe, G.J., 1999. Evaluating the use of goodness-of-fit measures in hydrologic and hydroclimatic model validation. Water Resour. Res. 35 (1), 233–241.
Lewis, J., Shulman, I., Blumberg, A., 1998. Assimilation of Doppler radar current data into numerical ocean models. Cont. Shelf Res. 18 (5), 541–559.
Lipa, B., 2003. Uncertainties in seasoned current velocities. Proceedings of the IEEE/OES Seventh Working Conference on. IEEE, pp. 95–100.
Lipa, B., Whelan, C., Rector, B., Nyden, B., 2009. HF radar bistatic measurement of surface current velocities: Drifter comparisons and radar consistency checks. Remote Sens. 1 (4), 1190–1211.
Liu, Y., MacCready, P., Hickey, B., Dever, E., Kosro, P., Banas, N., 2009. Evaluation of a coastal ocean circulation model for the Columbia River plume in summer 2004. J. Geophys. Res. 114, C00B04.
Marmorino, G., Hallock, Z., 2001. On estimating wind velocity using an upward-looking ADCP. J. Atmos. Ocean. Technol. 18 (5), 791–798.
Mau, J.C., Wang, D.P., Ullman, D., Codiga, D.L., 2007. Comparison of observed (HF radar, ADCP) and model barotropic tidal currents in the New York Bight and Block Island Sound. Estuar. Coast. Shelf Sci. 72, 129–137.
May, P.W., 1979. Analysis and interpretation of tidal currents in the coastal boundary layer(Ph.D. thesis) Massachusetts Institute of Technology.
McCuen, R., Snyder, W., 1975. A proposed index for comparing hydrographs. Water Resour. Res. 11 (6), 1021–1024.
Mellor, G.L., Yamada, T., 1982. Development of a turbulence closure model for geophysical fluid problems. Rev. Geophys. Space Phys. 20 (4), 851–875.
Moore, D., Notz, W., 2010. Statistics: Concepts and controversies. W. H. Freeman.
Moustafa, M.Z., Hamrick, J.M., 1994. Modelling circulation and salinity transport in the Indian River lagoon. In: Spaulding, M.L. (Ed.), 3rd International Conference on Estuarine and Coastal Modeling. American Society for Civil Engineers, New York, pp. 381–395.
Munchow, A., Garvine, R.W., 1993. Buoyancy and wind forcing of a coastal current. J. Mar. Res. 51, 293–322.
Ng, B., 1993. The prediction of nearshore wind-induced surface currents from wind velocities measured at nearby land stations. J. Phys. Oceanogr. 23 (8), 1609–1617.
Nolan, G.D., 1997. A study of the river Corrib plume and its associated dynamics in Galway Bay during the winter months(Master's thesis) University College Galway.
O'Donncha, F., Ragnoli, E., Suits, F., 2014. Parallelisation study of a three-dimensional environmental flow model. Comput. Geosci. 64, 96–103.
O'Donnell, J., Ullman, D.S., Spaulding, M., Howlett, E., Fake, T., Hall, P., Isaji, T., Edwards, C., Anderson, E., McClay, T., Kohut, J.T., Allen, A., Lester, S., Lewandowski, M., 2005. Integration of Coastal Ocean Dynamics Application Radar (CODAR) and Short-Term Prediction System (STPS) surface current estimates into the Search and Rescue Optimal Planning System (SAROPS), U.S. Coast Guard Tech. Rep., DTCG39-00-DR00008/HSCG32-04-J-100052.
Padman, L., Erofeeva, S., 2004. A barotropic inverse tidal model for the Arctic Ocean. Geophys. Res. Lett. 31 (2) L02303.
Paduan, J.D., Washburn, L., 2013. High-frequency radar observations of ocean surface currents. Ann. Rev. Mar. Sci. 5, 115–136.
Pawlowicz, R., Beardsley, B., Lentz, S., 2002. Classical tidal harmonic analysis including error estimates in matlab using t_tide. Comput. Geosci. 28 (8), 929–937.
Pidgeon, E., Winant, C., 2005. Diurnal variability in currents and temperature on the continental shelf between central and southern California. J. Geophys. Res. 110, C03024.

Port, A., Gurgel, K., Staneva, J., Schulz-Stellenfleth, J., Stanev, E., 2011. Tidal and wind-driven surface currents in the German Bight: HFR observations versus model simulations. Ocean Dyn. 1–19.
Prandle, D., 1987. The fine-structure of nearshore tidal and residual circulations revealed by HF radar surface current measurements. J. Phys. Oceanogr. 17, 231–245.
Prandle, D., 1997. Tidal and wind-driven currents from OSCR. Oceanography 10 (2), 57–59.
Prandle, D., Loch, S.G., Player, R., 1993. Tidal flow through the Straits of Dover. J Phys Oceanogr 23 (1).
Price, J.F., Weller, R.A., Schudlich, R.R., 1987. Wind-driven ocean currents and Ekman transport. Science 238 (4833), 1534–1538.
Rabinovich, A., Shevchenko, G., Thomson, R., 2007. Sea ice and current response to the wind: A vector regressional analysis approach. J. Atmos. Ocean. Technol. 24 (6), 1086–1101.
Ragnoli, E., Donncha, F., Hartnett, M., 2012. Characterizing ocean gyres formation within a bay using vorticity and HF radar measurements. EGU General Assembly Conference Abstracts volume 14, p. 10684.
Rio, M., Hernandez, F., 2003. High-frequency response of wind-driven currents measured by drifting buoys and altimetry over the world ocean. J. Geophys. Res. 108 (3283), 10–1029.
Schmidt, R.O., 1986. Multiple emitter location and signal parameter estimation. IEEE Trans. Antennas Propag. 34 (3), 276–280.
Shen, J., Boon, J.D., Kuo, A.Y., 1999. A modeling study of a tidal intrusion front and its impact on larval dispersion in the James River Estuary, Virginia. Estuaries 22 (3), 681–692.
Smagorinsky, J., 1963. General circulation experiments with the primitive equations, part I: The basic experiment. Mon. Weather Rev. 91 (3), 99–164.
Smith, S.D., 1988. Coefficients for sea surface wind stress, heat flux, and wind profiles as a function of wind speed and temperature. J. Geophys. Res. Oceans (1978–2012) 93 (C12), 15467–15472.
Song, Y., Haidvogel, D., 1994. A semi-implicit ocean circulation model using a generalized topography-following coordinate system. J. Comput. Phys. 115 (1), 228–244.
Stewart, R.H., Joy, J.W., 1974. HF radio measurements of surface currents. Deep-Sea Res. I 21 (12), 1039–1049.
Taylor, P., Yelland, M., 2001. The dependence of sea surface roughness on the height and steepness of the waves. J. Phys. Oceanogr. 31 (2), 572–590.
Teague, C., Vesecky, J., Hallock, Z., 2001. A comparison of multifrequency HF radar and ADCP measurements of near-surface currents during COPE-3. IEEE J. Ocean. Eng. 26 (3), 399–405.
Ullman, D.S., O'Donnell, J., Kohut, J., Fake, T., Allen, A., 2006. Trajectory prediction using HF radar surface currents: Monte Carlo simulations of prediction uncertainties. J. Geophys. Res. 111 (14 PP.).
Warner, J.C., Sherwood, C.R., Arango, H.G., Signell, R.P., 2005. Performance of four turbulence closure models implemented using a generic length scale method. Ocean Model 8 (1–2), 81–113.
Weisberg, R., Li, Z., Muller-Karger, F., 2001. West Florida shelf response to local wind forcing: April 1998. J Geophys Res, C. J. Geophys. Res. C: Oceans 106 (C12), 31239.
Wheeler, A.J., Monteys, X., 2010. Atlas of the deep-water seabed: Ireland. Springer.
Wilkin, J., 2006. The summertime heat budget and circulation of southeast new england shelf waters. J. Phys. Oceanogr. 36 (11), 1997–2011.
Wilks, D., 2011. Statistical methods in the atmospheric sciences. volume 100. Academic press.
Willmott, C., 1981. On the validation of models. Phys. Geogr. 2 (C5), 184–194.
Willmott, C.J., Robeson, S.M., Matsuura, K., 2012. A refined index of model performance. Int. J. Climatol. 32 (13), 2088–2094.
Yaremchuk, M., Sentchev, A., 2009. Mapping radar-derived sea surface currents with a variational method. Cont. Shelf Res. 29 (14), 1711–1722.
Yaremchuk, M., Sentchev, A., 2011. A combined EOF/variational approach for mapping radar-derived sea surface currents. Technical Report; Stennis Space Center, MS, 39529. Naval Research Laboratory.
Yoshikawa, Y., Masuda, A., Marubayashi, K., Ishibashi, M., Okuno, A., 2006. On the accuracy of hf radar measurement in the tsushima strait. J. Geophys. Res. Oceans (1978–2012) 111, C4.
Yoshikawa, Y., Matsuno, T., Marubayashi, K., Fukudome, K., 2007. A surface velocity spiral observed with ADCP and HF radar in the tsushima strait. J. Geophys. Res. 112 (14 PP.).